X-Ray photoelectron and Raman Studies of Microwave Plasma Assisted Chemical Vapour Deposition (PACVD) diamond films

Bernard Humbert, Nesrine Hellala, Jean Jacques Ehrhardt, Silvère Barrat, Elizabeth Bauer-Grosse

X-Ray photoelectron and Raman Studies of Microwave Plasma Assisted Chemical Vapour Deposition (PACVD) diamond films

Bernard HUMBERT[2*], Nesrine HELLALA[1], Jean Jacques EHRHARDT[2], Silvère BARRAT[1] and Elizabeth BAUER-GROSSE[1]

1. Laboratoire de Science et Génie des Surfaces, LSGS, UMR 7570 CNRS-Nancy-University, Ecole des Mines de Nancy CS14234, Parc de Saurupt 54042 Nancy Cedex (France)
2. Laboratoire de Chimie Physique et Microbiologie pour l'Environnement, LCPME, UMR 7564 CNRS-Nancy-University, 405, rue de Vandoeuvre, 54600 Villers lès Nancy (France)

* Corresponding author humbert@lcpme.cnrs-nancy.fr

Key words: diamond films, XPS, Raman, internal stresses
Chemical vapour deposition, Diamond, X-ray spectroscopy, Raman spectroscopy, stress measurements, coatings

Abstract:

X-ray photoelectron and Raman spectroscopies were used to investigate the chemical and the structural properties of thin diamond films synthesised by Plasma Assisted Chemical Vapour Deposition (PACVD). This powerful combination expanded the chemical physics understanding of CVD diamond continuous films, during the first stages of growth that determine the global diamond film quality. Two peculiar properties were studied (i) the stress measurements were discussed by distinguishing clearly the chemical effects from the mechanical effects; (ii) an electronic gap at 2.7 eV probed by Raman resonance that

corresponds to an energy loss peak on the XPS carbon signal, was related to the surface hydrogenation.

1. Introduction:

Since three decades, a lot of interest has been focused on synthetic diamond synthesized by Plasma Enhanced Chemical Vapour Deposition (PECVD) process. It is due to the perspective of large number of technological developments linked to multiple diamond properties which can be associated each others. In the case of its functional properties such as its transparency to visible light, high carrier mobilities, high breakdown field or chemical inertness, a lot of applications are envisaged in the domain of radiation detectors, optoelectronic devices, spectral windows, heat sinks, MEMS systems or diamond-based microelectronic components [1]. Excepted for homoepitaxial diamond synthesis where the film is a quasi-single crystal, many works are devoted to CVD diamond synthesis on cheaper substrates than diamond as single silicon substrates. The main objective is the production of low-cost and high quality diamond films usable in technological components. However due to high interfacial energy between diamond nuclei and silicon substrates as well as the plasma-diamond interaction, the growth occurs by islands and the polycrystalline nature of the subsequent diamond coatings induces the formation structural defects like grain boundaries, stacking faults which damage functional properties and produce internal stresses. Moreover, the interaction between the plasma discharge (created from the gas excitation by external energy source) and the growing diamond surfaces leads to the formation of non diamond carbonaceous components (as graphite or amorphous carbon phases) or insertion of non carbon atoms (as hydrogen or nitrogen). Since fifteen years ago, Highly Oriented Diamond (HOD) films have been prepared thanks to the Yugo's method [2] of Bias enhanced Nucleation (BEN). If bias and experimental conditions of the BEN step are adequate, we generally observe a partial epitaxial nucleation which strongly decreases the structural defects inside the subsequent growing film [3] but some problems remain unresolved as the poor epitaxial ratio, the azimuthal misorientation and the lack of nucleation reproducibility [6 4 5]. Moreover, the physico-chemical properties of HOD films strongly depend on the diamond growth chemistry that is very difficult to understand due to the very complex plasma/surface interactions in these PECVD processes [7]. The most used plasma-producing gas is CH_4/H_2 mixture with a very large percentage of hydrogen whose chemical effects are fundamental but

not completely determined, in particular the consequence of the hydrogen chemisorption on the crystalline diamond growth [8]. Additional introductions of other gases inside the discharge have been studied to modify the plasma chemistry and consequently to vary the physico-chemical properties of the films. Nitrogen, argon and oxygen are the most frequent gases and particularly oxygen that strongly modifies the growth rate, the diamond deposition domain and the global quality of the diamond due to a direct interaction with the chemisorbed hydrogen [11 9 10 4]. Therefore $CH_4/H_2/O_2$ gas mixtures were used in this work to synthesize the diamond films. XPS (X-ray Photoelectron Spectroscopy) and micro confocal Raman spectroscopy, were jointly used to investigate the surface and the bulk as well, in parallel with SEM (scanning electron microscopy) and XRD (X-ray diffraction). Therefore some insight in the chemical and structural information on these films could be obtained and used to better understand their properties in relation to the gas composition.

Many XPS studies have been reported recently dealing with the purity of diamond films especially on the content of sp^2 carbon in the diamond structure [12], the structural changes and the modifications of the electronic structure induced by atom beam or ion bombardment [14 13], the mechanism of growth of the films [15], and so on. Despite it has been recognised since a long time that XPS is a suitable technique to characterise the surface of diamond films [14] the surface characterisation of this material by this technique remains a very difficult task for several reasons:

- The first one relies on the difficulty of calibrating the energy scale of the XPS spectrometers when analysing an insulating or semi-conducting material for which the standard procedures cannot be used due to the absence of a possible internal reference such as aliphatic carbon coming from adventitious carbon. Therefore the values reported in the literature for the binding energy for the C1s level on diamond are usually ranging from 283.3 to 285.0 eV [14 13 14]. If the surface Fermi level of diamond is used and if a band gap energy of 5.5eV is considered, then the C1s binding energy for diamond surface would be located around 289.2 eV [16]. Fortunately, the presence of some donor states of hydrogen-terminated diamond surface improves considerably the surface conduction properties of the diamond films deposited on conducting materials making safer the measurement of the C1s binding energies. Therefore, the most recent studies indicate a trend towards binding energies of C1s around or below 284.0 eV for diamond [16 17 18 19].
- The second one is dealing with the impossibility of cleaning this type of material by classical cycles of ion sputtering and annealing. Surface damage, incorporation of

argon ions and also the irreversible transformation of sp^3 carbon atoms into sp^2 carbon atoms make the ion surface cleaning procedures absolutely not usable. Therefore meaningful and reliable XPS results for diamond, graphite and amorphous carbon materials can only be obtained with a clean and intact surface sample [20].

- Finally, as XPS is a surface sensitive technique, the chemical information could also contain some unexpected elements coming for example from the process of termination of the films such as adsorption of elements of the plasma during the cooling down.

From its early beginnings, Raman spectroscopy has been recognized to be ideally suited to diamond study [21]. During the last two decades, innumerable Raman works have been obtained either isolated diamond crystallites or continuous films [for example 23 22]. The Raman spectra may be used to study residual stress in diamond deposition [24] or to characterise diamond polytypes [25] or yet to study the crystallographic orientation of isolated chemical vapour deposited microcrystals [22]. The backscattered Raman spectra of the [111] and [100] directions of micrometric isolated CVD diamond crystals revealed significant differences. The observed splitting of the 1332 cm^{-1} diamond line into three bands around 1326, 1334 and 1340 cm^{-1} has been detailed in minute thanks to polarisation measurements [22]. The 1326 cm^{-1} component is only observed when sampling a {111} growth sector and is strongly polarisation sensitive. Stuart et al. [22] assumed that this peak originates from the non-uniform distribution of {111} stacking faults throughout the {111} sectors of the crystal. Recently, the confocal Raman microspectrometry has been also successfully used to study thin films deposited either silicon or diamond substrates [23]. Indeed, the confocal Raman microspectrometry allowed the mapping, at a micrometric scale, of the local stresses existing in the diamond films. For instance, in the case of high quality freestanding polycrystalline boron-doped diamond films, 2D stress or defect images were deduced from the Raman spectra. Both compressive and tensile stresses were thus measured within diamond grains, in particular close to defects or grain boundaries.

In this study we will report on high resolution XPS and Raman investigations of continuous PECVD diamond films produced in various $CH_4/H_2/O_2$ gas mixtures where the plasma discharge was obtained by a microwave excitation (MPCVD process). We will focus on the chemical purity and on the local textural and structural properties, measured simultaneously on the same sample with various analysis depths of continuous polycrystalline

diamond films whose nucleation was initiated by a BEN pre-treatment. This one guaranties us a high nucleation density inducing the formation of continuous coatings having relatively low thicknesses. We will discuss the complementary features of both measurements, to describe the MPCVD films. In particular, the effect of the hydrogenation of any kinds of faces will be envisaged to interpret the Raman spectral evolutions with the wavelength of the laser excitation.

2. Materials and methods

Polycrystalline diamond films have been grown on silicon by MPCVD technique using a BEN step for the nucleation and a growth step for the film formation. Details of deposition parameters in a 2.45-GHz microwave plasma CVD reactor will be found in previous papers [26 27]. Briefly, a Si(100) wafer substrate of 10 by 10 mm previously chemically cleaned in acetone and deoxidized in a solution of hydrofluoric acid is attached on a molybdenum sample holder. The total pressure and the total flow rate in the reactor were respectively fixed at 30 hPa and 300 sccm. The gas composition was basically varied between 0.8-1 vol.% of methane in hydrogen. Oxygen (about 0.5-1 vol.%) was introduced in the gas phase. The BEN stage was performed by negatively biasing the silicon substrate up to 250V relative to the plasma discharge and the microwave power was maintained at 300W during the BEN and growth steps leading to a substrate temperature close to 750°C. The growth step duration was usually between 4 to 5 hours. Table 1 summarises the synthesis parameters of each run and the measured thickness of the corresponding samples.

The microstructure, morphology and thickness of each sample were checked by XRD (Bragg-Brentano diffractometer, using a Co Kα incident radiation.) and SEM (Philips XL 30 SFEG) techniques.

The XPS analyses were carried out with a Kratos Axis Ultra (Kratos Analytical, UK) spectrometer with a hemispherical energy analyser and using a monochromatic AlKα source (1486.6 eV). As the delay-line detector allows a high count rate the power applied to the X-ray anode was reduced to 90 W so that the possible X-ray induced degradation of the sample was minimized. The instrument work function was calibrated to give a binding energy (BE) of 83.96 eV for the Au 4f7/2 line for metallic gold and the spectrometer dispersion was adjusted to give a BE of 932.62 eV for Cu 2p3/2 line for metallic copper.

The samples were attached to the sample holder and then evacuated overnight prior analyses. The pressure in the analysis chamber during XPS analysis was in the low 10^{-9} hPa range. All spectra were recorded at a 90° take-off angle, the analysed area being currently about 700 μm^2. Survey spectra were recorded with 1.0 eV step and 160 eV analyser pass energy and the high resolution regions with 0.05 eV step and 20 eV pass energy (instrumental resolution better than 0.5 eV). In both cases the hybrid lens mode was employed. As the various samples studied here behave as conducting materials, the charge neutraliser was never used and the binding energies have not been corrected.

Spectra were analysed using the Vision software from Kratos (Vision 2.2.6). A Shirley base line allows the subtraction of the background whereas Gaussian G (60%) Lorentzian L (40%) peaks or asymmetrical GL peaks were used for spectral decomposition. As the analysed samples were not grown *in situ* in the XPS analysis chamber, they were inevitably exposed to atmospheric conditions during the transfer from the deposition system to the XPS analysis chamber.

Raman spectra were recorded with a triple substractive monochromator T64000 Jobin Yvon spectrometer equipped with a confocal microscope. The detector was a charged coupled device (CCD) cooled by liquid nitrogen. The Raman spectra were excited by a laser beam at 514.53 nm, 488 nm and 457 nm emitted by an Argon Laser (Stabilite 2017, Spectra Physics), focused on samples with a diameter of about 0.8 μm and a power of about 20 mW on the sample. The Raman backscattering was collected through the microscope objective (x 100, numerical aperture of 0.95) and dispersed by a 1800 groves/mm grating to obtain 2.7, and 3.2 cm^{-1} spectral resolutions for respectively the 514.53 and 457 nm excitation beams. The wavenumber accuracy in vacuum was better than 0.8 cm^{-1}. The polarization discrimination of the optical device was checked by measuring the depolarization ratios for the perfectly known bands of reference liquid pure products. For instance, the experimental depolarization ratio for the 459 cm^{-1} symmetric component of the CCl_4 spectrum is 0.02 ± 0.005 for the different wavenumber positions of the centered CCD camera or 0.03 ± 0.01 for the C-H stretching mode of CH_2Cl_2. The confocal Raman microprobe is constituted by an Olympus microscope, equipped with a motorized XY stage with a step of 80 nm. On a test sample, a calibration gold grids on a silicon substrate, the experimental lateral resolution value is measured from the displacement necessary to pass from the maximum collected signal to the minimum at the boundaries of an object. The application of this convention to estimate the resolution of our

conventional confocal device gave the values of 700 nm and 550 nm for respectively the 514.53 and 457 nm excitation wavelengths. The theoretical description of the optical diffraction applied to a perfect Gaussian laser beam and a perfect optical device would give respectively 270 and 250 nm [28 29] for the lateral resolution and 800 and 700 nm for the axial resolution. However, let us note that, because of the high refractive index of diamond, this axial resolution is damaged and values are about multiplied by a factor of about 2. Thus the smaller analyzed volume by our confocal device may be estimated at around 0.350 μm^3 and the more current volume in our experiments will be around 1 μm^3.

3. Experimental results

3.1 Structural characterisation of the films

Figure 1 displays both planar and cross-sectional SEM views for the three samples A, B, C and their corresponding diffraction patterns. The three diamond films exhibit well-shaped grains with emerging {100} and {111} facets which have grown on the silicon substrates to form continuous films. Although the mean grain size of sample B is smaller than for sample C, their surface morphologies are comparable showing numerous cuboctahedral crystals with <110> direction normal to the substrate characteristic of a <110> fibre axis. However, that one is better formed for sample C than sample B. The surface morphology of sample A is quite different presenting rather a bimodal diamond crystal size distribution characteristic of an evolutionary selection rule in progress (fibre axis not yet formed). The SEM cross-section views of the three diamond films show that the growth rate of sample C is clearly higher than the two others ones that explains the presence of a well formed fibre axis. The observed difference concerning the fibre axis formation and growth rate can be explained by the variations of methane and oxygen concentrations [9 10], by the variations of growth duration and by the fact that identical BEN conditions induces slight nucleation densities [5]..

XRD patterns show the most intense signal comes from the (400) silicon reflection and three peaks characteristic of the (111), (220) and (311) diamond reflections. The relative intensities for these latest ones indicate that no preferential orientation seems to be detected for sample A, whereas a <110> fibre axis is clearly observed for sample B and slightly accentuated for sample C according to the observed morphology. The presence of preferential orientation for sample B which is not detected for sample A having the same thickness as sample B could be explained by a lower nucleation density for sample A which delays the

formation of the fibre axis [5]. Finally, the grain sizes observed for the three samples are small enough to consider that the area probed by the XPS spectrometer or by our microRaman device includes between ten and hundred grains. Moreover, since the three films are continuous, we will consider in the following that both the XPS and vibrational analyzes give average characterizations on the films and are unable to distinguish spatial heterogeneous parameters. Due to high spatial resolution of Raman analysis, we collected several spectra of different sample areas.

3.2 Reference samples for XPS and Raman

As we planed to analyse the C1s line observed on the as-grown diamond films it was necessary to obtain a coherent basis of binding energies for the possible contributions that could be encountered on these samples. It is widely accepted that C1s binding energy of amorphous carbon is fixed to 284.6 eV. Likewise the oxidised forms of carbon give rise to components at higher binding energy ranging from 286.0 to 289.5 eV depending of the net atomic charge of the carbon atom. In particular oxygen atom induces shifts to higher binding energy by about 1.5 eV per C-O bound [30]. However, the binding energy of sp^2 versus sp^3 carbon atom is still under debate, some authors [31] concluded that all pure C species, regardless the hybridisation have the same C1s binding energy while others postulated a separation of about 0.8 eV between the sp^2 and sp^3 contributions [16]. Most of the time the sp^3 configuration is reported to present a lower binding energy for C1s than the sp^2 contribution but, sometimes, the reverse situation has been reported [14 32],

Therefore, three samples, namely a synthetic diamond IIa type (Drukker International, crystal of 0.7 mm of size), a piece of freshly cleaved HOPG graphite and a sample of SiC (given by M.J. Ledoux LMSPC Strasbourg - France) have been characterized. The latter one is justified because it has been previously reported that diamond films growth on silicon wafers proceeds trough an interfacial SiC phase [15]. Graphite and pure diamond will be used as references for C1s line in the hybridisation states sp^2 and sp^3, respectively. The XPS C1s lines for these three samples are exhibited in figure 2. These peaks have been decomposed when it was necessary. Therefore, the binding energy, the FWHM's (full width half maximum) and the shape of each component are reported in table 2 for the three samples.

It is widely accepted that the C1s peak of graphite presents a very particular dissymmetric shape with a broadening on its high energy side [33 34 35]. This shape usually occurring in conductive materials is attributed to neutralization of the holes created during

photoemission by conduction electrons and the asymmetry is believed to be more pronounced when the density of state (DOS) at the Fermi level is high. Thanks to the ability of creating electron hole pairs in graphite and despite a rather low DOS at the Fermi level graphite exhibit a pronounced asymmetry. Therefore an asymmetric Gaussian Lorentzian shape has been used to fit the shape of the C1s peak in figure 1b. It is worth noting that on this sample a single narrow (FWHM = 0.77 eV) peak is observed at a binding energy of 284.18 eV with only a tenuous contamination component at 286.33 eV attributed to pollution after cleavage. The value reported here is in full agreement with the value given in the most recent papers of 284.3 ± 0.2 eV [16].

As diamond is a semiconductor, the choice of the shape C1s peaks for this material is less straightforward. A symmetric shape was reported previously [14] but, after many attempts, the best fit of the C1s peak presented in figure 2a was obtained with an asymmetric shape. This could tentatively be related to the conductive properties of this hydrogen-terminated diamond surface. Let us recall that no obvious charge effect was detected on this sample. Within this hypothesis, the C1s line for the diamond reference sample was deconvoluted in three components, the main one at 283.9 eV (FWHM = 0.87 eV) attributed to diamond, one at lower binding energy (283.26 eV) that will be attributed to SiO_xC_y (see below) and a third one at higher binding energy (286.0 eV) coming from adsorption on the sample of oxidised forms of carbon.

The C1s spectrum presented in figure 2c for SiC is rather complicated despite a soda treatment at 80°C that was supposed to remove the oxidised phases present on the surface [36]. The low binding energy component pointed out at 281.31 eV (FWHM = 1.16 eV) is assigned without ambiguity to the carbide whereas the four other components are related to oxycarbide, adventitious carbon and oxidised forms. The Si2p levels have also be observed for this sample (not shown here) and the binding energy for the Si2p3/2 level has been pointed out at 98.92 eV. Therefore the difference in energy between the Si2p3/2 level and the C1s level is found equal to 182.39 eV for SiC in agreement with previously reported values (182.17 ± 0.03 eV [37], 182.20± 0.1 eV [38] and 182.25 [15]) and giving then some confidence on our determination.

The backscattered Raman spectrum of the reference diamond sample is displayed in figure 3a. The spectrum is dominated by a very narrow peak centred at 1332.5 cm^{-1}. The Raman signal is strongly symmetric and the full width is smaller than 3.8 cm^{-1}. As expected, the cubic diamond with the 3C structure is revealed by the triply degenerated only Raman active

mode. This observation is in agreement with the phonon band diagram of this kind of crystal where the longitudinal and transverse optic phonon branches meet at 1332 cm^{-1} and represent one triply degenerate Raman mode at the centre of the Brillouin zone. Let us note that this crystal structure with two atoms per unit cell induces no first order infrared activity

The group theory applied to the symmetry of graphite, D_{6h}^4 shows that the reduction of the atomic movement representation at the zone centre yields 12 vibrational modes with nine optical phonons:

$$\Gamma_{opt} = 2E_{2g} \oplus E_{1g} \oplus 2B_{2g} \oplus A_{2u},$$

where only the two E_{2g} modes are Raman active. One of these two phonons is due to in-plane atomic displacements, the other to the rigid layer displacements. The first wavenumber characteristic of both the Raman active modes is found at 1581 cm^{-1}, the second at 42 cm^{-1}. Figure 3b displays the major first order at 1581 and second order at 2450, 2690, 2725 and 3247 cm^{-1}. The presence of both the components around 2700 and the sharpness of the 3247 cm^{-1} peak allow claiming a structurally well stacked sample [39 40]. A single peak at 2700 cm^{-1}, resulting of a coalescence of the doublet 2695 and 2725 cm^{-1} would be an evidence of a total lack of c-axis order, *i.e.*, a true disorder of the graphitic crystallinity. The absence of a large component around 1350 cm^{-1}, interpreted as a fingerprint of the finite size of graphene layers [40 41], confirms the large domain of the graphene plane of our sample.

The reference SiC (3C structure with the *F*43m structure or T_d^2) sample is characterised by the two sharp Raman peaks at 968 and 790 cm^{-1} assigned to the LO and TO phonons displayed on the recorded unpolarised spectrum of the figure 3c.

3.3 Characterisation of MPCVD diamond films

The XPS analysis of the surface of the three films does not reveal huge differences. The survey spectra (not shown here) are largely dominated, as expected, by the signal of C with traces of Si and O. The C1s spectra and the enhanced bottom of this peak of three samples are presented in figure 4. Looking first at the (C) sample it is observed that the C1s peak is largely dominated by a component located at a binding energy of 283.4 eV (FWHM = 0.98 eV) in full agreement with the accepted value for sp^3 C hybridisation. Furthermore it has to be pointed out that this spectrum is even of a better quality than our reference on pure diamond. The modelling of the bottom of the C1s peaks has been performed with four components associated with the presence of (i) carbon atoms in a SiO_xC_y environment

(282.35 eV) of (ii) C-H bounds (284.6 eV) and also of (iii) two other forms of C (286.0 and 288.35 eV). The parameters used for decomposition of the C1s line are presented in table 2. Sample (B) presents the highest percentage (around 8%) of the component C-H. The environment SiO_xC_y, observed for each sample, is probably coming from the oxygenated-species formed in the $CH_4/H_2/O_2$ plasma leading to additional incorporation into the (sub)-surface [42]. The component at 286.0 eV will be discussed below in light of the resonant feature observed in the Raman analysis. It could be due either to oxidised carbon or to an energy loss peak. Due to its low intensity a possible interpretation of the last component would be some spurious adsorption of oxidised compounds during the storage and the transfer of the samples.

The general Raman spectra obtained at 514.53 and 457 nm distinguish clearly the film C from the two others (figure 5). Indeed, in agreement with the thickness of the deposited films, the relative intensity of the diamond signal by comparison with the silicon Raman signal is about 20 time more intense for the film C than for the films A and B. Moreover, the luminescence coming from the volume of the layer is more intense for the thicker sample. The photoluminescence spectra excited at 457 or 514.53 nm do not present any sharp signal at neither 2.156 eV, nor 1.945 eV. Since the 2.156 eV signal is characteristic of an optical centre comprised of a single nitrogen atom while the one at 1.945 eV corresponds to vacancies trapped at single substitutional nitrogen atoms [43] we conclude that the concentration of nitrogen atoms in the volume is very low for the three samples, as at the surface analysed previously by XPS. The weak emission signal recorded for samples A and C at 1.681 eV is reported to be generated by optical centres due to the incorporation of silicon atoms during growth. This observation is in agreement with the surface analysis since it has to be pointed out that Si atoms have been unambiguously detected by XPS, presumably in an environment SiO_xC_y.

The three Raman spectra display the characteristic diamond line at around 1334 cm^{-1} , the characteristic signal of the silicon substrate crystallised in the cubic structure at 521 cm^{-1} and a broad band between 1500 and 1650 cm^{-1}, that corresponds to vibration modes of amorphous carbon with carbon atoms in sp^2 hybridisation. This last phase does not correspond however to a graphitic phase since no usual second order signals between 2400 and 2800 wavenumbers is displayed (figure 3). By comparison with the diamond line, the importance of this amorphous carbon phase is relatively weaker for the sample B than for the samples A and C. No Raman signal of the SiC polytype has been detected.

The Raman diamond signal is detailed in the inset of the figure 5. The three Raman spectra excited at 514.53 nm (table 4) are characterised by a maximum around 1334 cm^{-1}. The thinnest film (sample A) spectrum presents a symmetrical band centred at 1333.5 cm^{-1} with a full width at half height smaller than 7 cm^{-1} and a weak component with a low ratio signal on noise at 1326 cm^{-1}, while the band for sample B is rather constituted by two components with a FWHH of 8 cm^{-1}. The diamond peak of the film C is the most symmetrical of the three spectra, centred at 1334 cm^{-1} with a FWHH higher than 9 cm^{-1}. The decompositions of these signals confirm this first survey (table 4). The comparison of both the inelastic scattering signals in the diamond spectral range shows that the excitation at 457 nm generates, at the highest wavenumbers, an asymmetrical profile of the diamond Raman peak that may be fitted by a component around 1340 cm^{-1} that is not observed with the green excitation (figure 6 and table 4). This supplementary component is the strongest for the sample B and quasi-absent for sample C. This wavelength dependent behaviour will be discussed in the next section with the help of the XPS analysis after discussion of the splitting of the diamond signal in two lines, at 1330 and 1334 cm^{-1}, that is observed with both the wavelength.

4. Discussion

As reported by some authors [24 44 45] the two components in the Raman spectrum excited at 514.53 nm can be assigned to a partial lifting of the triply degenerated optical phonon T_{2g} at the Brillouin zone centre. This partial splitting of the two components respectively located at lower (1330 cm^{-1}) and higher (1334 cm^{-1}) wavenumbers could be assigned to the singlet (s) and doublet (d) phonons in the case of biaxial stress in the diamond films [46]. Indeed, in the presence of strain the cubic symmetry is lowered. Depending on the direction of the stress relative to crystallographic directions, the degeneracy may be partially or completely lifted. Let us note that this lifting of the degeneracy occurs for uniaxial or biaxial crystallographic strains but not for hydrostatic strains. As a general trend, an up-shift of the diamond Raman lines is observed with respect to the natural diamond position, ω_0, indicating the existence of a compressive stress. If we assume that our deposited films are in a biaxial in-plane stress, as reported by Ager and Drory [24], the biaxial stresses given for the two lifted levels can be expressed by the relationships:

$$\sigma_s = -1.08(\omega_s-\omega_0) \qquad \sigma_d = -0.384(\omega_d-\omega_0), \qquad \text{(eq.1)}$$

where ω_s and ω_d correspond to the observed wavenumbers of the single and the doublet in the spectrum and ω_0 the stress-free peak position of the diamond line, while the σ_s and σ_d represent the related biaxial stresses (expressed in GPa).

The residual stress in the diamond films arises from the superposition of a thermal and an intrinsic components. The thermal stress originates from the difference in the thermal expansion coefficients of silicon and diamond. As a result of this difference, the silicon substrate contracts more than the diamond films upon cooling down to room temperature, hence a compressive stress applies on the diamond film. The intrinsic stress component in the diamond film arises mainly from impurities and defects, such as grain boundaries, twins, dislocations, voids and amorphous carbon incorporated during the diamond growth. In particular, compressive intrinsic stress in the films is ascribed to impurities; while defects, such as vacancies, dislocations and grain boundaries, produce tensile intrinsic-stress. In the case of the morphology of our samples displayed by the electronic microscopy (figure 1), the area probed by the microRaman device is constituted by several ten of grains. Consequently, the Raman shifts and the band widths between 7 and 10 wavenumbers, correspond to a convolution or a distribution of these different effects since no individual grain may be distinguished here. To probe individual grains, the Raman analysis of the optical near field excited or collected by a subwavelength tip [28] would have to be applied. Therefore in the case of the sample spectra for which the splitting is not obvious, we rather adopt the approach already used for instance by Donato et al. [46] that used the relationship proposed by Ralchenko et al. [47] to evaluate the biaxial stress:

$$\sigma = -0.567(\omega_m - \omega_0) \qquad \text{(eq.2)}$$

where the measured peak position is the medium between the singlet and the doublet wavenumbers:

$$\omega_m = 0.5(\omega_s + \omega_d) \qquad \text{(eq.3)}.$$

Thus, as initially proposed by Donato et al. [46] to estimate the overall film stress, the last equation (eq.3) may be adapted to our case. The value of ω_m is estimated from the average wavenumber measured in our thin films (between 200 and 2000 nm) representative of the grain distribution. This assumption applied to the case of the film C gives a stress of -1.134 GPa in agreement with the trend analyzed by Donato for thicker films. This trend indicates that the biaxial in-plane stress in diamond films gradually decreases with increasing film

thickness, as expected from the theory of elasticity [48]. However, the distribution is more complex in our case as evidenced by the highest FWHH value (about 9 cm^{-1} against 4 or 7 for the Donato et al. results).

This trend is not fully representative of the thinnest films A and B. The film B spectra display clearly two components that may be analyzed with the help of equations (1), showing a compressive and a tensile stresses. If we use the corresponding values of ω_s=1330 cm^{-1}, ω_d=1334.8 cm^{-1} and ω_0=1332 cm^{-1}, we obtain the biaxial stresses σ_s = +2.16 GPa and σ_d = -0.97 GPa. Let us note that the impurity concentrations are the lowest for the film B (absence of the 1.681 eV luminescence signal [49], no colour centre attached at the nitrogen substitutions in the bulk and the lowest concentration of silicon atoms at the surface probed by XPS). Consequently the observed splitting for the Raman diamond line of sample B may be interpreted from a strict mechanical point of view, including the boundary and the stacking faults effects. When the rapid growth by formation of a <110> fibre axis symmetrically generates in-plane internal stresses [50], particularly along the <100> and <111> directions, the difference of stress sign (compressive for σ_s and tensile for σ_d) for <110> oriented diamond crystals is attributed to either the grain boundary structure of <110> oriented films or a non uniform distribution of defects inside the crystals [51]. This behaviour is associated to a highly heterogeneous strain field arising from the most dominant planar structural defects such as twins and stacking faults [44]. Compressive stresses of one GPa magnitude are reported in the {111} growth sectors where planar defects are present. They are balanced by tensile stress in {100} growth domains exempt of bidimensional defects but they can contain voids and dislocations which generate tensile stresses [52]. For samples B and C, the formation of <110> fibre axis induces non isotropic stresses along the <100> and <111> directions belonging to the diamond film plane.

The macroscopic stress is difficult to appreciate since it corresponds to the combination of intrinsic and thermal stresses. The thermal stress is compressive in the case of diamond film on silicon and the intrinsic stress is tensile in nature [53 54]. Kim and Yu [54] observed that the compressive stress was measured for low film thicknesses. Knowing that the thermal stress is more prominent for thin films [55 56], sample B could be more compressively stressed than sample C since the diamond thickness strongly increases from sample B to sample C. The stress drops from compressive for small thickness to tensile for high film thickness. This point could allow us to explain first the more resolved splitting observed for the sample B than for C (table 4 and figures 5 and 6) and second a higher up-

wavenumber observed for B than for C. Nevertheless the stress values estimated from the previous equations are not so easy to compare, since in the case of the film B, the splitting is easily resolved while for the film C is difficult to be determined. The highest chemical quality of the film C than the ones of the films B observed either at the surface by XPS analysis or in the bulk by the luminescence does not seem to have consequence on these mechanical properties.

The randomly oriented crystals characteristic of sample A (fig. 1), with no preferential crystallographic direction are characterized by a weak component around 1326 cm^{-1} and a symmetrical component at 1333.5 cm^{-1}, with a relative low FWHH value in comparison with the other films (Table 4). No Raman splitting is observed in this disordered film contrary to the oriented B film. The 1326 component is related to the stacking faults that cause a breakdown in the symmetry without reaching a hexagonal structure. The appearance of this band is due to the non-uniform distribution of film A. The other component at 1333 cm^{-1} corresponds to the usual diamond mode under a weak compressive stress.

The previous discussion about the splitting of the Raman active diamond modes applies also here for the excited 457 nm Raman spectra since the same contributions are obtained at 1330 and 1334.5 cm^{-1}. However, for the samples A and B, a supplementary component at 1340 cm^{-1} appears with this violet excitation. The Raman spectrum for the sample C is weakly affected by the wavelength change. This spectral response could be related to a particular carbon structure that possesses a Raman enhancement when the wavelength is 457 nm (i.e. 2.7 eV). Indeed if the electronic state of this particular structure is characterised by a band gap smaller than 3 eV, the laser excitation is able to generate a Raman resonance effect. The Raman efficiency is multiplied by a factor of three to six orders of magnitude in comparison with the usual Raman effect. In our three films, the sample B is the most representative of this kind of structure. The only noticeable difference of this sample with the others comes from its chemical composition of surface displayed by the XPS analysis (table 3). The surface concentration of the CH environment is the highest (table 3) and concomitantly the component around 286.2 eV is the highest. Thus we propose that the possible Raman resonance effect generated at 2.7 eV observed strongly for the sample B could be produced by the electronic structure generated by the C-H composition present at the surface. The gap around 2.7 eV is also displayed on the carbon XPS spectrum by a component at the binding energy of 286.2 eV, that may be assigned to an energy loss peak at (286.2-283.5) eV. This XPS component is consequently not assigned to an oxidised environment of

carbon atoms (C=O) but rather to a consequence of this gap specific to a surface reconstruction of some faces. This assignment is in agreement with theoretical predictions computed on (100)(2x1) partially hydrogen covered surfaces [56] and experimental observations from anisotropy optical reflectance [57]. This assignment is confirmed by analysing the two other films. Indeed, the film A surface, characterized by a smaller H concentration than B (table 3), possesses a weaker component at 286.2 eV too and presents a weaker Raman resonance effect with the 457 nm excitation (table 4). More convincing, the Raman spectrum of the more perfect diamond film C excited in the violet is similar to the signal excited in the green without any resonance effect while the components at 286.2 eV and 284.5 eV binding energy are negligible in its XPS spectrum (table 3) confirming the absences of hydrogen termination and the surface electronic gap.

5. Conclusions

This paper presents a double spectroscopic approach to understand CVD diamond continuous thin films of thickness ranging between 300 nm and 2 µm. This approach is fundamental to further optimize the global diamond quality (in terms of chemistry and structure) in the first stage of growth. The whole results are obtained thanks to a concomitantly fundamental spectroscopic analysis of reference samples. The powerful combination of X-ray photoelectron and Raman spectroscopies is revealed in the chemical physics understanding of CVD diamond continuous films. This potential is applied to investigate two peculiar properties (i) the stress measured in CVD films is interpreted by distinguishing clearly the chemical effects from the mechanical effects; (ii) the electronic gap at 2.7 eV, is probed by a resonance effect on the Raman signal that corresponds to an energy loss peak on the XPS carbon signal. The origin of this gap for some thin continuous films is due to a peculiar surface H termination evidenced by the fined analysis of the XPS carbon signal. Further investigations will be envisaged to more precisely characterise the stress development for very thin diamond films and the coupled effect of hydrogen/oxygen in relation to the electronic surface properties.

Acknowledgment: The authors would like to thank J. Lambert from LCPME for the acquisition of the XPS spectra.

References

1. A.A. Altukhov, M.S. Afanas'ev, V.B. Kvaskov, V.E. Lyubchenko, A. Yu. Mityagin, E.N. Murav'ev, L.A. Pomortsev, V.A. Potapov, B.V. Spitzyn, Inorganic Materials 40 (2004) 50
2. S. Yugo, S. Kanai, T. Kimura, T. Muto, Appl. Phys. Lett. 58 (1991) 1036
3. N. Bozzolo, S. Barrat, I. Dieguez, E. Bauer-Grosse, Diamond Relat. Mater. 6 (1997) 41
6. J.C. Arnault, Surface Review Letters, 10:1 (2003) 127
4. S.T. Lee, Z. Lin, X. Jiang, Materials Science and Engineering, 25 (1999) 123
5. S. Saada, S. Barrat, E. Bauer-Grosse, Diamond Relat. Mater. 9 (2000) 300
7. P.W. May, Phil. Trans.R. Soc. Lond. A 358 (2000) 473
8. H. Kawarada, Surface Science Report 26 (1996) 205
11. C.J. Tang, A.J. Neves, A.J. Fernandes, Diamond Relat. Mater. 13 (2004) 203
9. M. Frenklach, H. Wang, Phys. Rev. B, 43:2 (1991) 1520
10. R. Beckmann, S. Reinke, M. Kuhr, W. Kulisch, R. Kassing, Surf. Coat. Technol., 60 (1993) 506
12 K.G. Saw, J. du Plessis, Materials Letters 58 (2004) 1344
14. J. I. B. Wilson, J. S. Watson, G. Beamson, J. of Electron Spectroscopies and related Phenomena 121 (2001) 183
13. J.F. Morar, F.J. Himpsel, G. Hollinger, J.L. Jordan, G. Hughes, F.R. McFeely, Phys. Rev. B 33 (1986) 1340
15. L. Demuynck, J.C. Arnault, R. Polini, F. Le Normand, Surface Science 377-379 (1997) 871
16. G. Speranza, N. Laidani, Diamond Relat. Mater. 13 (2004) 445-450 and 451-458 and references cited therein
17. P. Reinke, G. Francz, P. Oehlhafen, J; Ullmann, Phys. Rev. B 54 (1996) 7067
18. S. Dieckhoff, D. Ochs, J. Günster, V. Kempter, Surface Science 423 (1999) 53
19W. M. Lau, L. J. Huang, I. Bello, Y. M. Yiu, S.T. Lee, J. Appl. Phys. 75 (1994) 3385
20. Y. Fan, A.G. Fitzgerald, P. John, C.E. Troupe, J.I.B. Wilson, Surface Interface Analysis 34 (2002) 703
21. D.S. Knight, W.B. White, J. Mater. Res. 4 (1989) 385
23. M. Mermoux, A. Tajani, B. Marcus, E. Bustarret, E. Gheeraert, M. Nesladek and S. Koizumi, Diamond Relat. Mater., 13 (2004) 886
22. K.E. Stuart, S. Prawer, P.S. Weiser, Diamond Relat. Mater. 2 (1993) 753
24. J.W. Ager, M.D. Drory, Phys. Rev. B 48 (1993) 2601
25. K.E. Spear, A.W. Phelps, W.B. White J. of Mater. Res. 5 (1990) 2277
26. S. Barrat, S. Saada, J.M. Thiebaut, E. Bauer-Grosse; Diamond Relat. Mater. 10 (2001) 1637
27. I.H. Choi, S. Barrat, E. Bauer-Grosse; Diamond Relat. Mater. 12 (2003) 362
28. J. Grausem, B. Humbert, M. Spajer, D. Courjon, A. Burneau and J. Oswalt, J. Raman Spectrosc. 30 (1999) 833
29. J. Barbillat, P. Dhamelincourt, M. Delhaye and E. Da Silva, J. Raman Spectrosc. 25 (1994) 3.
30. D. Briggs and M.P. Seah in " Practical surface Analysis" Volume 1 : Auger and X-ray Photoelectron Spectroscopy 2nd Edition , John Wiley and Sons Ltd, Editor (1994)
31. D.N. Belton and S.J. Schmieg J. Vac. Sci.Technol. A8 (1990) 2353
32. A. Ermolieff, A. Chabli, F. Pierre, G. Rolland, D. Rouchon, C. Vanuffel, C. Vergnaud, J. Baylet and M.N. Semeria, Surf. Interf. Anal. 31 (2001) 185
33. P.M. Th. M. van Attekum and G.K. Wertheim Phys. Rev. Letters 43 (1979) 1896
2834. F. Sette, G.K. Wertheim, Y. Ma, G. Meigs, S. Modesti, C.T. Chen, Phys. Rev. B 41 (1990) 9766

35. H. Estrade-Szwarckopf, Carbon 42 (2004) 1713
36. N. Keller, C. Pham-Huu, M.J. Ledoux, C. Estournes, G. Ehret, Applied Catalysis A : General 187 (1999) 255
37. T.M. Parril, Y.W. Chung, Surface Science 243 (1991) 96
38. A. Guise, J.C. Arnault, S. Saada, S. Barrat, E. Bauer-Grosse, Diamond Relat. Mater., submitted
39. R. Al-Jishi and G. Dresselhaus, Phys. Rev. B 26 (1982) 4514
40. H. Wilhem, E. McRae, F. Lelaurain and B. Humbert, J. Appl. Phys. 84:12, (1998) 6555
42 W. Deferme, K. Haenen1, G. Tanasa, C. F. J. Flipse, M. Nesládek, phys. stat. sol. (a) 203:12 (2006) 3114
41. F. Tuinstra and J.L. Koenig, J. Chem. Phys. 53 (1970) 1126
43 G. Davies and M.F. Hamer, Proc. R. Soc. London, A 348 (1976) 285
49 A.T. Collins, Diamond and Related Materials 1 (1992) 457
44. H. Windischmann, K.J. Gray, Diamond Relat. Mater. 4 (1995) 837
45. M. Yoshikawa, G. Katagiri, H. Ishida, A. Ishitani, M. Ono and K. Matsumura, Appl. Phys. Lett., 55 (1989) 2608
46. M. G. Donato, G. Faggio, M. Marinelli, G. Messina, E. Milani, A. Paoletti, S. Santangelo, A. Tucciarone and G. Verona Rinati, Diamond Relat. Mater. 10 (2001) 1535
47 V.G. Ralchenko, A.A. Smolin, V.G. Pereverzev et al., Diam. Relat. Mater. 4(1995) 754.
48 Q–H. Fan, A. Fernandes, E. Pereira and J. Grácio, Diamond Relat. Mater. 8 (1999) 645
50. J.W. Steeds, A.E. Mora, S.J. Charles, D.J.F. Evans, J.E. Butler, Materials Chemistry and Physics, 81 (2003) 281
51. I. I. Vlasov, V. G. Ralchenko, E. D. Obraztsova, A. A. Smolin and V. I. Konov, Thin Solid Films, 308-309 (1997) 168
52. K. H. Chen, Y. L. Lai, J. C. Lin, K. J. Song, L. C. Chen and C. Y. Huang., Diamond Relat. Mater. 4 (1995) 460
53. H. Windischmann et al. J. Appl. Phys. 69:4 (1991) 2231
54. J.G. Kim and J. Yu, Scripta Materiala, 36 (1998) 807
55. S. R. Sails, D. J. Gardiner, M. Bowden, J. Savage, and S. Haq, Appl. Phys. Lett., 65 (1994) 43
56. B.N. Davidson and W.E. Pickett, Phys. Rev. B, 49 (1994) 11253
57. V.I. Gavrilenko and A.I. Shkrebtii, Surface Sci. 324 (1995) 226

Tables

Table 1: CVD growth parameters and corresponding diamond thicknesses for samples A, B and C

Sample	**A**	**B**	**C**
Duration (h)	5	4	5
H_2 vol.%	98.7	98.2	98.5
CH_4 vol.%	0.8	0.8	1
O_2 vol.%	0.5	1	0.5
Thickness (nm)	300	400	2200

Table 2: Decomposition parameters of the C1s peaks obtained on the three reference samples and presented in figure 2

	C1s component (eV)	Fwhm eV	Shape	Assignation
Diamond IIa	283.26 (15%)	1.45		?
	283.90 (77.5%)	0.87	AS (75 ; 0.6)	C sp3
	286.0 (7.5%)	2.65		Oxidised carbon or satellite structure
Graphite	284.18 (93%)	0.775	AS (80 ; 0.5)	C sp2
	286.33 (7%)	1.86		Oxidised carbon
SiC	281.31 (50%)	1.16	AS (75 ; 0.6)	SiC
	282.01 (9%)	1.33		SiO_xC_y
	284.55 (31%)	1.54		C aliphatic
	285.68 (6%)	2.02		Oxidised carbon
	287.85 (4)	2.00		Oxidised carbon

Table 3: XPS analysis of the C1s line on the three MPCVD diamond films

Environments	Film (A)	Film (B)	Film (C)
SiO_xC_y (282.7 eV)	3 %	0.5 %	1 %
C diamond (283.4 eV)	89 %	86 %	96 %
C-H (284,5 eV)	2 %	8 %	1 %
C-O or satellite structure (286 eV)	4 %	3.5 %	1 %
C=O (288 eV)	2 %	2 %	1 %

Table 4: Proposed decompositions for the Raman spectra of the three films excited by both the wavelengths 514.53 and 457 nm.

	Green excitation			Violet excitation		
Samples	Positions (cm^{-1})	FWHH (cm^{-1})	Percent	Positions (cm^{-1})	FWHH (cm^{-1})	Percent
Film (A)	1325 1333.5	12 7	10% 90%	1326 1335 1339.5	10 7 7	10% 77% 13%
Film (B)	1330 1334.8	5.5 5.5	30% 70%	1329 1335 1340	4 7 6	8% 74% 18%
Film (C)	1330 1334	8 8	10% 90%	1331 1334 1340	7 9 4	9% 89% 2%

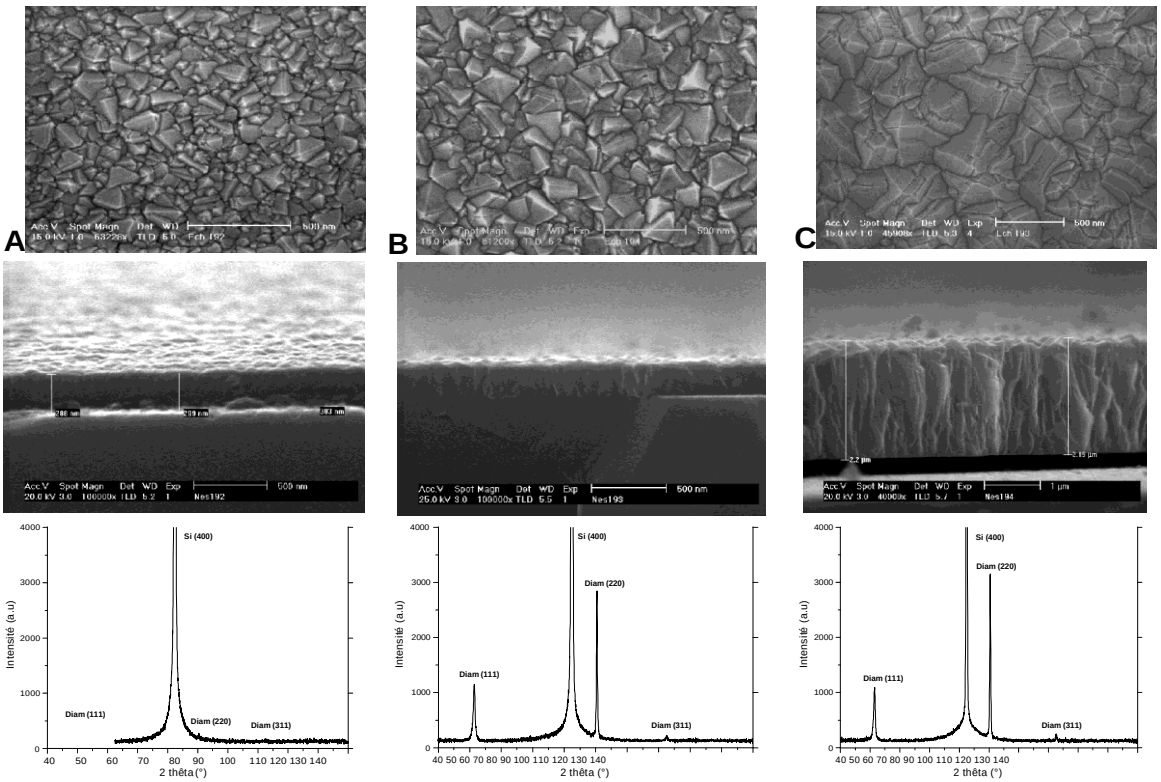

Figure 1: Planar and cross sectional SEM views of the three samples and their corresponding diffraction patterns.

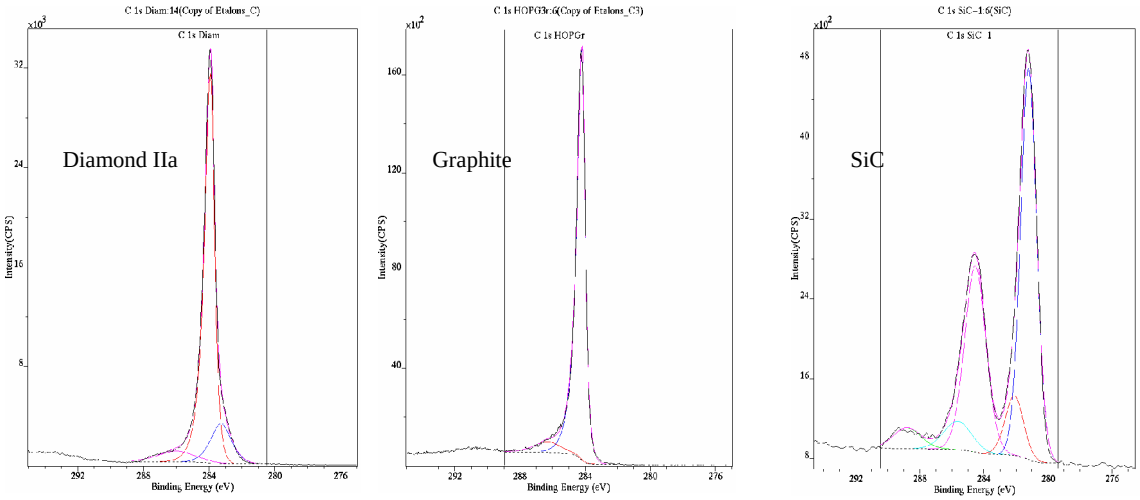

a b c

Figure 2: C1s XPS spectra of (a) diamond IIa, (b) freshly cleaved HOPG graphite and (c) α-SiC. It is worth noting that neither ion sputtering nor charge neutraliser has been used for the analysis of all these samples. A contamination layer is clearly evidenced on the sample of SiC, but as long as we are mainly interested in the determination of the binding energy of C1s in SiC and SiO_xC_y, the components associated to these phases are sufficiently shifted to be analysed safely.

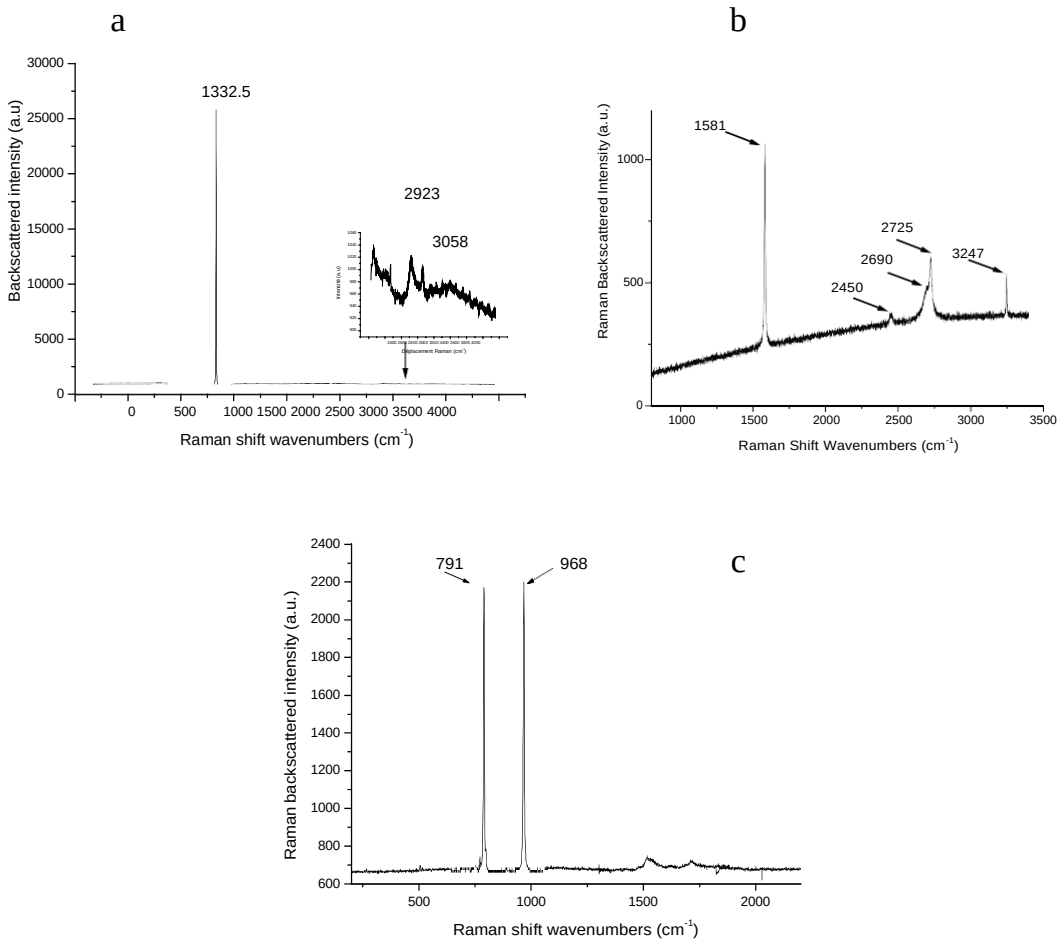

Figure 3: Backscattered Raman spectra of (a) diamond IIa (b) freshly cleaved HOPG graphite and (c) SiC. The spectra are excited at 514.53 nm. The microscope objective used is a dry objective (X 100) with a numerical aperture of 0.95. Each of the first order signals may be decomposed by a single symmetric lorentzian curve.

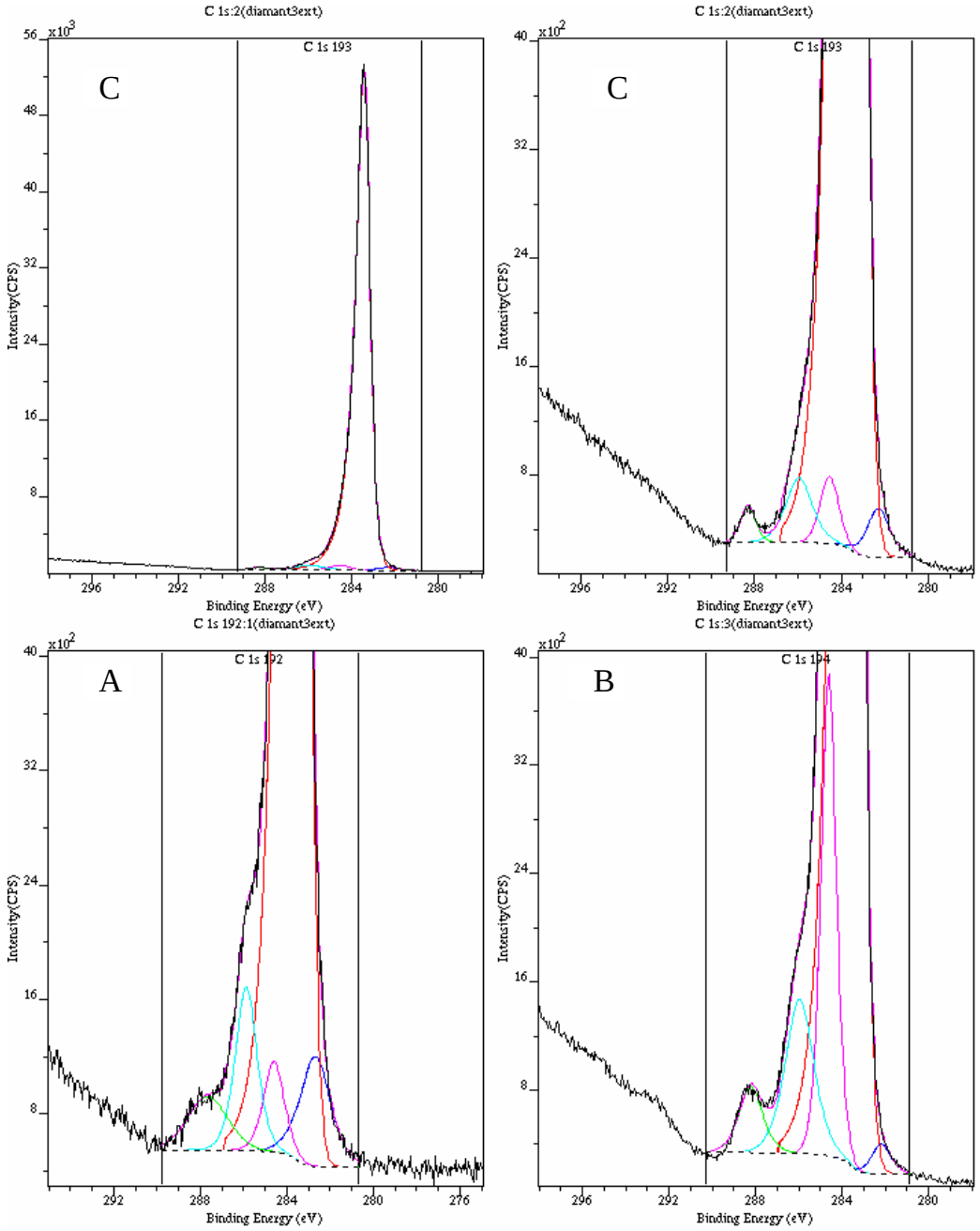

Figure 4: C1s XPS spectra of the diamond films A, B and C grown on Si(100). On the top the C1s peak of film C is presented, the Y axis being also expanded (upper right) in order to show the small components that could be evidenced in the bottom of the main C1s peak. For films A and B the presentation has been restricted to the zoomed bottom of the C1s peak. It is worth noting that the intensities of the C-H (284.5 eV) and of the energy loss (286.0 eV) components are much more pronounced on samples A and B.

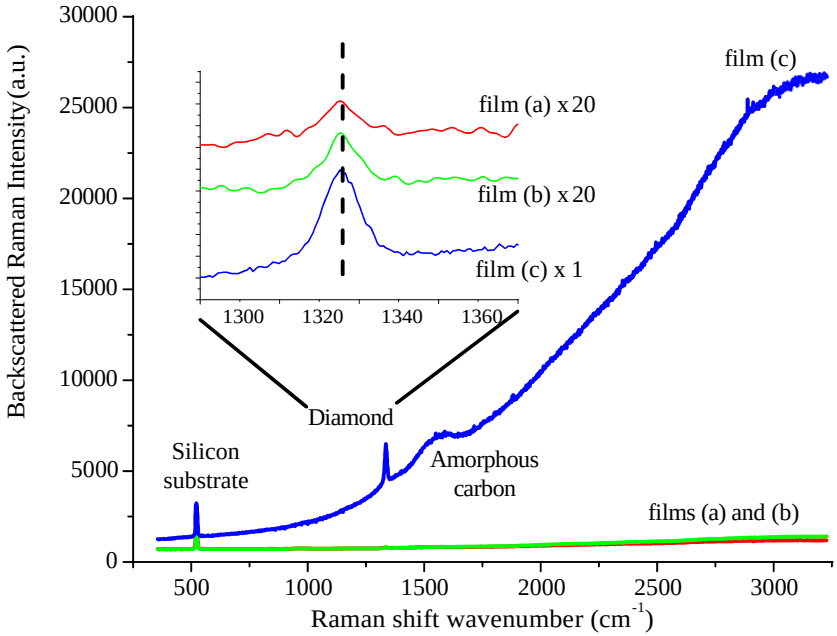

Figure 5: Raman spectra of the three samples recorded with the same integration time. The spectrum of the film (C) makes it seem quite different from (A) and (B) by the relative intensity of the "background" luminescence, by the relative strong intensity of the diamond Raman signal and by the weakest signal of the silicon Raman signal. The spectra are recorded with an excitation at 457 nm. The inset displays zoomed spectra around the diamond signal.

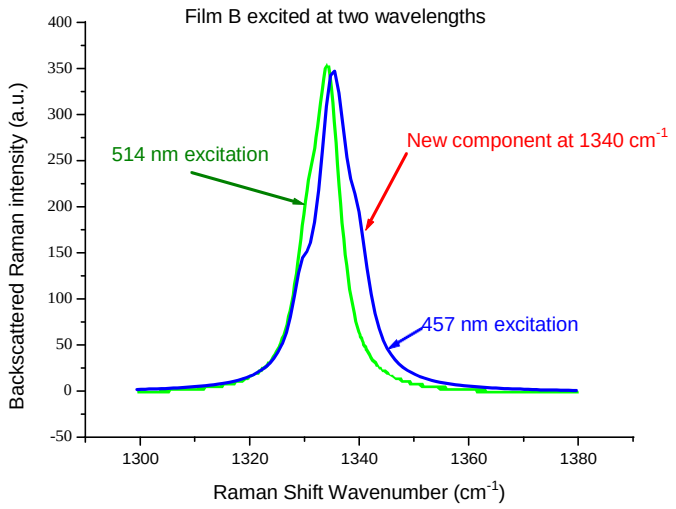

Figure 6: Comparison of both the spectra of film B excited, in blue at 457 nm and excited in green at 514.53 nm. This phenomenon is the strongest for this film that displays the highest concentration of hydrogen at the surface (table 3).

Figure(s)

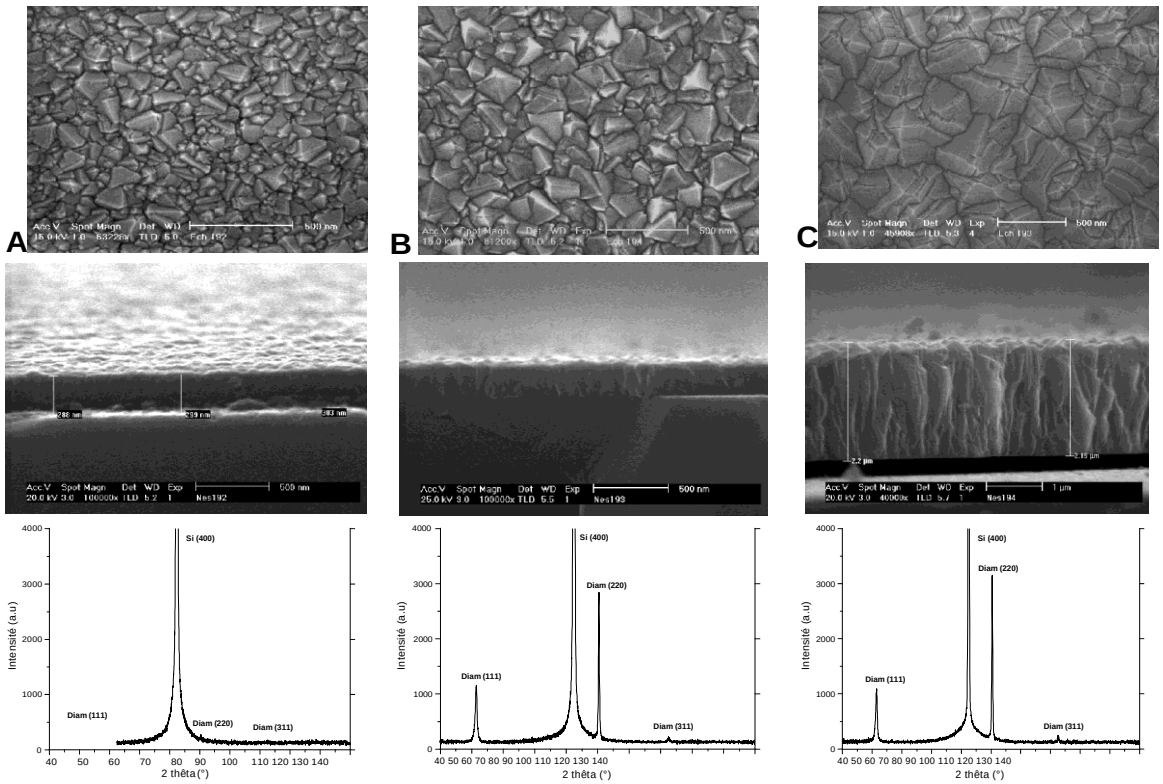

Figure 1: Planar and cross sectional SEM views of the three samples and their corresponding diffraction patterns.

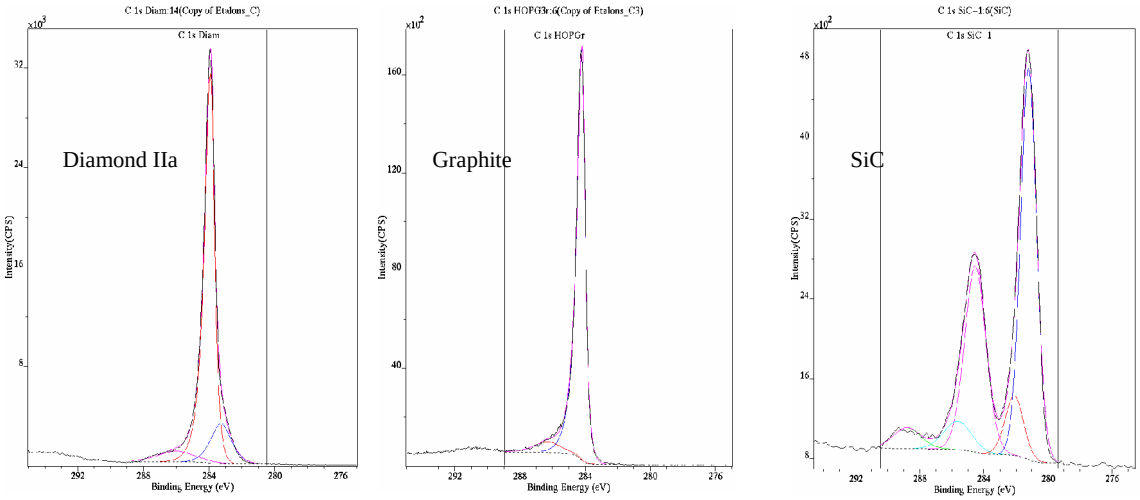

a b c

Figure 2: C1s XPS spectra of (a) diamond IIa, (b) freshly cleaved HOPG graphite and (c) α-SiC. It is worth noting that neither ion sputtering nor charge neutraliser has been used for the analysis of all these samples. A contamination layer is clearly evidenced on the sample of SiC, but as long as we are mainly interested in the determination of the binding energy of C1s in SiC and SiO_xC_y, the components associated to these phases are sufficiently shifted to be analysed safely.

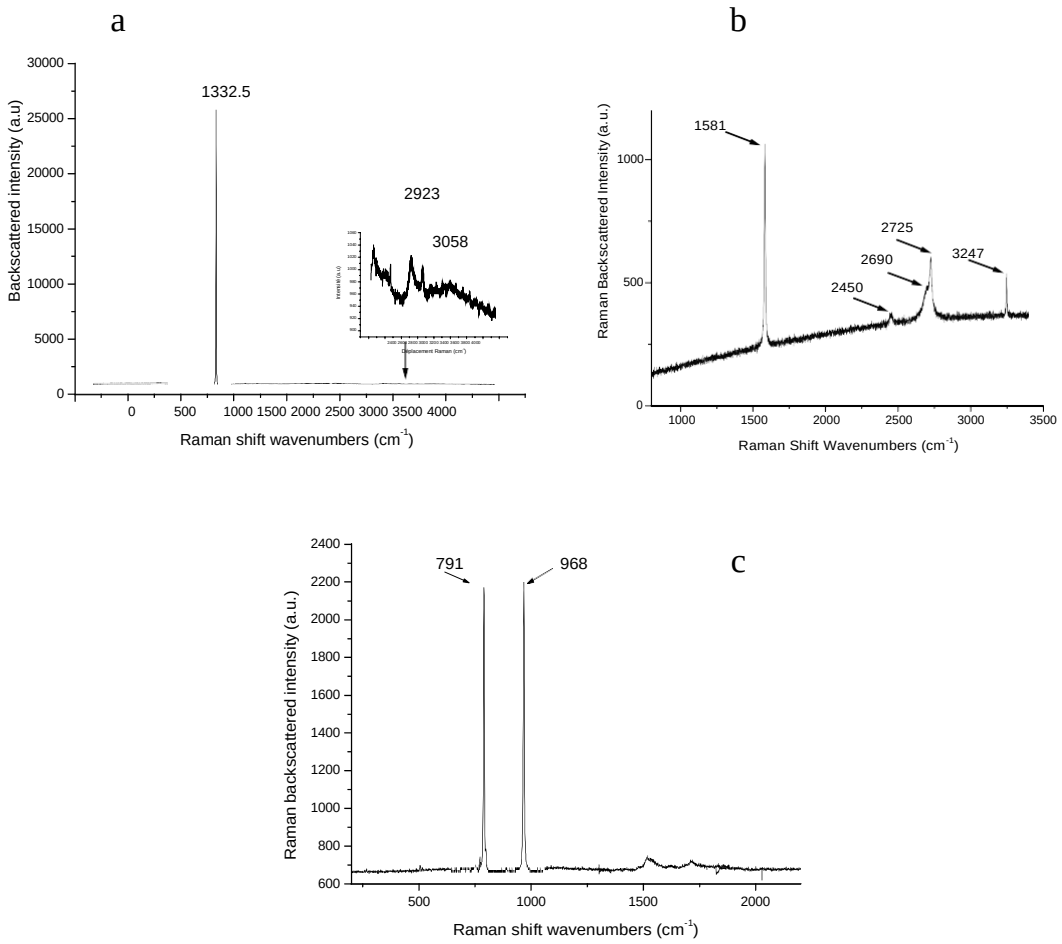

Figure 3: Backscattered Raman spectra of (a) diamond IIa (b) freshly cleaved HOPG graphite and (c) SiC. The spectra are excited at 514.53 nm. The microscope objective used is a dry objective (X 100) with a numerical aperture of 0.95. Each of the first order signals may be decomposed by a single symmetric lorentzian curve.

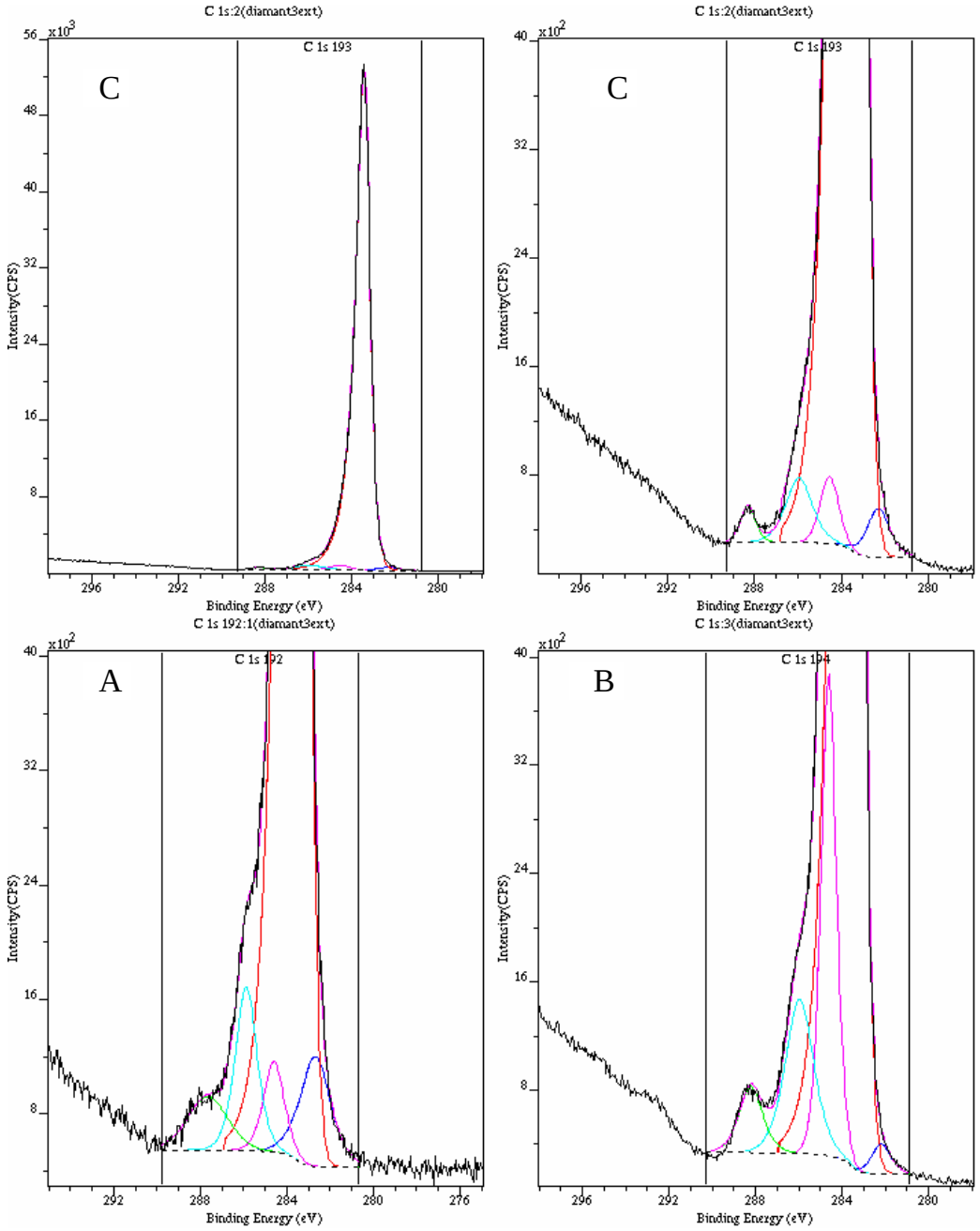

Figure 4: C1s XPS spectra of the diamond films A, B and C grown on Si(100). On the top the C1s peak of film C is presented, the Y axis being also expanded (upper right) in order to show the small components that could be evidenced in the bottom of the main C1s peak. For films A and B the presentation has been restricted to the zoomed bottom of the C1s peak. It is worth noting that the intensities of the C-H (284.5 eV) and of the energy loss (286.0 eV) components are much more pronounced on samples A and B.

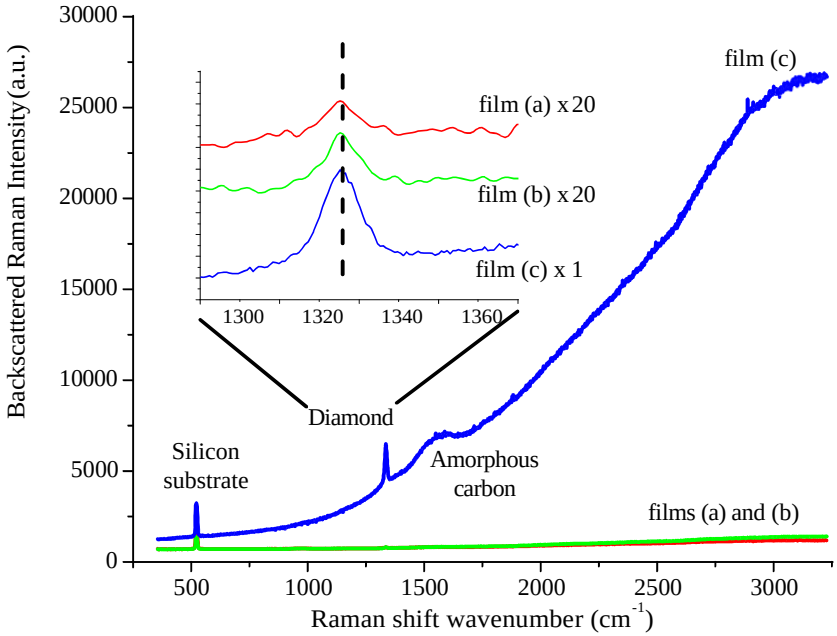

Figure 5: Raman spectra of the three samples recorded with the same integration time. The spectrum of the film (C) makes it seem quite different from (A) and (B) by the relative intensity of the "background" luminescence, by the relative strong intensity of the diamond Raman signal and by the weakest signal of the silicon Raman signal. The spectra are recorded with an excitation at 457 nm. The inset displays zoomed spectra around the diamond signal.

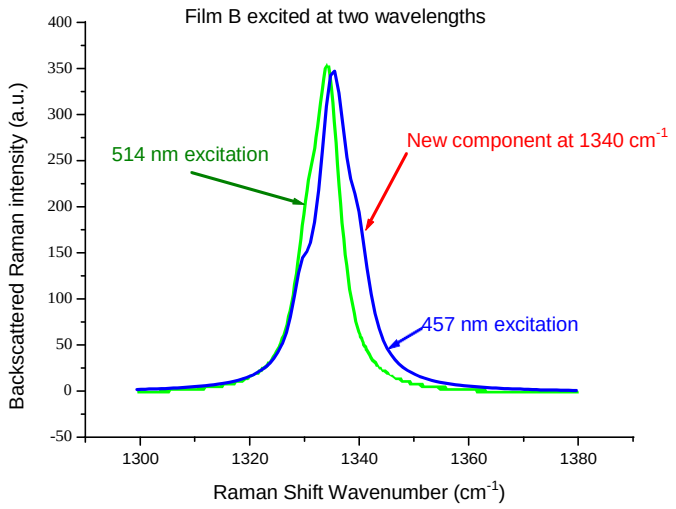

Figure 6: Comparison of both the spectra of film B excited, in blue at 457 nm and excited in green at 514.53 nm. This phenomenon is the strongest for this film that displays the highest concentration of hydrogen at the surface (table 3).

Tables

Table 1: CVD growth parameters and corresponding diamond thicknesses for samples A, B and C

Sample	**A**	**B**	**C**
Duration (h)	5	4	5
H_2 vol.%	98.7	98.2	98.5
CH_4 vol.%	0.8	0.8	1
O_2 vol.%	0.5	1	0.5
Thickness (nm)	300	400	2200

Table 2: Decomposition parameters of the C1s peaks obtained on the three reference samples and presented in figure 2

	C1s component (eV)	Fwhm eV	Shape	Assignation
Diamond IIa	283.26 (15%)	1.45		?
	283.90 (77.5%)	0.87	AS (75 ; 0.6)	C sp3
	286.0 (7.5%)	2.65		Oxidised carbon or satellite structure
Graphite	284.18 (93%)	0.775	AS (80 ; 0.5)	C sp2
	286.33 (7%)	1.86		Oxidised carbon
SiC	281.31 (50%)	1.16	AS (75 ; 0.6)	SiC
	282.01 (9%)	1.33		SiO_xC_y
	284.55 (31%)	1.54		C aliphatic
	285.68 (6%)	2.02		Oxidised carbon
	287.85 (4)	2.00		Oxidised carbon

Table 3: XPS analysis of the C1s line on the three MPCVD diamond films

Environments	Film (A)	Film (B)	Film (C)
SiO_xC_y (282.7 eV)	3 %	0.5 %	1 %
C diamond (283.4 eV)	89 %	86 %	96 %
C-H (284,5 eV)	2 %	8 %	1 %
C-O or satellite structure (286 eV)	4 %	3.5 %	1 %
C=O (288 eV)	2 %	2 %	1 %

Table 4: Proposed decompositions for the Raman spectra of the three films excited by both the wavelengths 514.53 and 457 nm.

	Green excitation			Violet excitation		
Samples	Positions (cm^{-1})	FWHH (cm^{-1})	Percent	Positions (cm^{-1})	FWHH (cm^{-1})	Percent
Film (A)	1325 1333.5	12 7	10% 90%	1326 1335 1339.5	10 7 7	10% 77% 13%
Film (B)	1330 1334.8	5.5 5.5	30% 70%	1329 1335 1340	4 7 6	8% 74% 18%
Film (C)	1330 1334	8 8	10% 90%	1331 1334 1340	7 9 4	9% 89% 2%